EUROPEAN ORGANIZATION FOR NUCLEAR RESEARCH

CERN–PH–EP/2005–30
21 June 2005

SPECTROSCOPY AND LIFETIME MEASUREMENTS OF STATES IN ^{76}KR POPULATED IN ^{76}RB DECAY

Abstract

The properties of the excited states of ^{76}Kr, populated in the decay of ^{76}Rb produced at ISOLDE isotopic separator, have been investigated by using K-conversion electron, γ-ray, and γ - γ coincidence measurements. The lifetimes of several levels have been measured by means of the Advanced Time-Delayed $\beta\gamma\gamma(t)$ method. The identification of 19 new levels and 55 transitions and the information deduced on spin and/or parity of the observed states from K-conversion coefficients, log *ft* values and decay properties have led to an improved knowledge of the level scheme. In particular, six 1^- states have been definitely identified and $J^\pi = 2^-$ has been assigned to the 2227 keV level, on which a band proposed to have negative-parity and even-spin had been previously observed. The strengths of the *E*0 and *E*2 transitions de-exciting the 0_2^+ and 0_3^+ states (the latter is here identified with the state at 1598 keV) have been measured. The experimental data concerning the 0_2^+ state have been analyzed in a simple two states mixing model and in the framework of the proton-neutron interacting boson model.

A. Giannatiempo[(1,2)], A. Nannini[(2)], A. Perego[(1,2)], P.Sona[(1,2)]
[(1)] Dipartimento di Fisica, Università di Firenze and
[(2)]Istituto Nazionale di Fisica Nucleare, Florence, Italy

H. Mach, B. Fogelberg
Department of Radiation Sciences, University of Uppsala, S-75121 Uppsala, Sweden

M.J.G. Borge, O. Tengblad, L.M. Fraile[♯)]
Instituto de Estructura de la Materia
Consejo Superior de Investigaciones Científicas, Madrid, Spain

A.J. Aas[♮)]
Department of Chemistry, University of Oslo, Blindern, Oslo, Norway

K. Gulda[♭)]
Department of Physics, University of Warsaw, Warsaw, Poland

and the ISOLDE collaboration

The IS317 and ISOLDE Collaborations

(Submitted to Phys. Rev. C)

1 INTRODUCTION

Over the past two decades even krypton isotopes have been the object of considerable experimental and theoretical attention due to the evolution of the nuclear structure, as a function of the neutron number and of the angular momentum, which displays collectivity modulated by shell effects. Microscopic calculations, performed using different models (see, e.g., [1–5]) predict a structural change of the equilibrium configurations along the krypton chain with coexistence of prolate and near-oblate or spherical shapes. On the other hand, the properties of positive parity states in the even krypton isotopes are correctly reproduced [6–10] by collective models based on the interacting boson approximation (IBA) [11]. One of the still open problems concerns the structure of the low-lying 0^+ states, whose study is of particular interest to clarify the contribution of the different excitation mechanisms at low energy. In the past years some of us have measured the *E*0 and *E*2 strengths [9, 12] of the transitions de-exciting the 0_2^+ state in ^{78,80}Kr. The recent identification of this state and the measurement of its *E*0 decay in ^{72}Kr [13] and in ^{74}Kr [14, 15] made it possible to complete the information on the 0_2^+ state from A=72 to A=82 [16] with the only exception of ^{76}Kr.

Concerning the states of negative parity, several bands have been observed all along the isotopic chain and an important theoretical effort has been devoted to their interpretation, whereas experimental information on levels not belonging to bands, which could help in understanding the structure of the states at low energy, is very scanty.

The aim of the present work was to experimentally investigate the isotope ^{76}Kr to provide new information on the decay of the 0_2^+ state and on states of negative parity, and to exploit the new data to study the nature of some levels of particular interest.

2 EXPERIMENT

In the experimental study [9, 12] of the 0_2^+ state in $^{78-80}$Kr the nucleus of interest was populated in the EC-β^+ decay of mass-separated parent nucleus $^{78-80}$Rb, produced at the ISOLDE facility at CERN. The same procedure has been utilized to feed the levels in ^{76}Kr. The ^{76}Rb [$T_{1/2}$ = 39 s] nuclei were produced in spallation reaction on a Nb-foil target by using the pulsed 1 GeV proton beam from the PS Booster and separated in the on-line mass separator.

Two separate experimental stations were located at the end of two ISOLDE beam lines. Spectroscopic information on the levels of ^{76}Kr were obtained by measurements of $\beta\gamma\gamma$ coincidences at the first station, which provided information on the $\gamma - \gamma$ coincidence relations and level lifetimes from the time-delayed spectra, while the second experimental station allowed to measure internal conversion electrons and singles-γ-ray spectra.

2.1 The fast timing station

The fast timing station utilized a set of four detectors positioned around the beam deposition point in a close geometry. The beam was implanted into a tape, which periodically carried away the old samples with long-lived activities and thus enhanced detection of transitions from the decay of ^{76}Rb. Unlike the rather standard fast timing setup for β^- decay spectroscopy, see [17, 18], where the ΔE β detector is positioned as close as possible behind the source and separated from the vacuum system by a thin Al foil, here the β detector was placed 1.8 cm further back and behind a conical lead shielding with walls 7 mm thick. The narrow opening

♯) Present address: *CERN, PH Department, CH-1211 Geneva 23, Switzerland.*
On leave from *Universidad Complutense, E-28006 Madrid, Spain.*
♮) Present address: *McKinsey & Company, Oslo, Norway*
♭) Present address: *Ministry of Economic Affairs and Labour Department of Innovation, Warsaw, Poland*

of the shield faced the tape. Its 13 mm diameter exceeded the diameter of the source, which was about 5-6 mm. The wider opening of the shield had 25 mm in diameter and faced the β detector. Its diameter exceeded that of the NE111A scintillator. This precaution was needed in order to eliminate as much as possible the presence of coincident 511 keV γ rays coming from disintegration of positronium, in a process following β^+ decay. Three γ detectors: two Ge spectrometers, with the relative efficiency of 40% and 60%, and one fast-response BaF_2 detector, 2.5 cm in length, were also used in the set-up.

Triple coincidence $\beta\gamma\gamma$ events were collected and analyzed off-line. These involved β-Ge-Ge and β-Ge-BaF_2 detectors. The latter was used for the lifetime determination, while the former provided $\gamma - \gamma$ relations, which allowed construction of the decay scheme and at the same time revealed the exact content of the coincident BaF_2 spectra. The analysis of this data set is discussed next.

2.1.1 $\gamma - \gamma$ coincidences

About 9×10^6 $\beta\gamma\gamma$ coincidences were collected involving the β-Ge-Ge detectors. The data were sorted out using gates set on various γ-ray transitions, which allow to verify the previous decay scheme and include a number of new levels and transitions. Figures 1-3 show various coincident spectra gated by γ-rays in the decay of ^{76}Rb to ^{76}Kr. In particular, Fig. 1 shows partial evidence for the new energy level at 2192 keV. A strong γ-ray cascade involving the 355-378-1768-424 keV transitions, depopulating known levels at 2926 and 2571 keV and feeding the known level at 424 keV, uniquely defines a new level at 2192 keV.

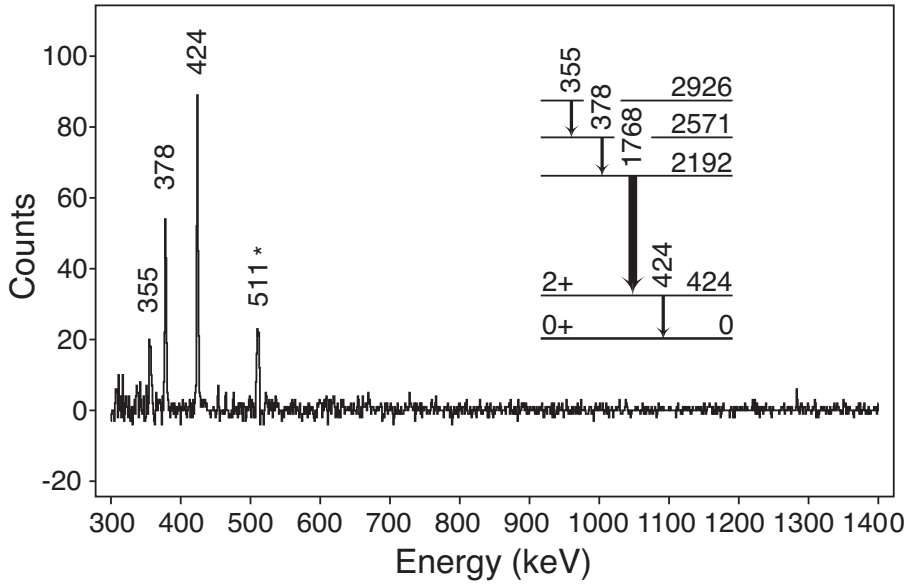

Fig. 1: Portion of the γ-ray spectrum in coincidence with the 1768-keV transition showing evidence for the new level at 2192 keV. It is an example of $\beta\gamma\gamma$ coincident spectrum recorded in two Ge detectors and gated by β-events. A partial decay scheme shown in the figure illustrates the position of the gating 1768 keV transition and the 355, 378 and 424 keV γ-rays. The latter de-excited known states in ^{76}Kr. The 511 keV peak is due to the β^+ decay process.

The sequence in which the 378 keV and 1768 keV transitions are placed in the cascade, 378-1768, is defined by the requirement of the intensity balance. Namely, the intensity of the 1768 keV line is twice as high as that for the 378 keV transition.

The results of the coincidence measurements allowed the identification of 19 new levels and the unambiguous placement of 53 transitions, as reported in Table I. The full discussion of the new level scheme is provided in Section III.

Table 1: Energies and intensities (in percentage of the intensity of the 424 keV, $2_1^+ \rightarrow 0_1^+$ transition) of the new gamma transitions placed in the level scheme of ^{76}Kr. In the first column the new levels identified in the present work are reported in italics.

E_{level}(keV)	E_γ(keV)	Relative Intensity	Coincident lines
1733.3	698.4	0.21(2)	424, 611
	511.6	0.5(3)	424, 494, 798
2091.4	493.4	0.21(7)	479, 1174
2104.3	882.4	2.4(5)	798, 822, 2185
	506.0	0.8(3)	822, 1174
	417.1	0.22(2)	346, 424, 917
2140.5	2140.5	0.31(3)	
	918.5	1.2(4)	798, 1222, 1463
2192.4	1768.4	1.07(6)	355, 378, 424
2227.2	540.0	0.24(2)	346, 424, 917
	493.8	0.7(2)	424, 798, 1309
2257.4	1222.6	0.9(5)	424, 611, 767
2332.6	2332.2	0.20(5)	1270
	1908.5	0.65(3)	424, 1270
2571.0	466.9	0.24(10)	424, 1680
	378.5	0.54(2)	424, 1768
2581.0	1546.1	0.42(17)	443, 611
	1359.4	0.90(4)	424, 443, 798, 1222
2700.4	2276.6	1.20(6)	324, 424
	1665.6	0.30(5)	324, 611
2742.3	1009.0	0.21(2)	424, 1309
2816.7	2046.5	0.81(6)	346, 424
2970.0	2546.0	1.13(7)	424
3024.2	1291.3	0.45(7)	424, 1309
	920.2	0.89(4)	346, 424, 882, 1680, 2104
	443.3	0.27(3)	424, 798, 1222, 1360, 2571
	324.3	0.77(4)	424, 611, 1665, 2276
3242.2	3242.3	1.2(2)	432
	2817.3	2.1(6)	424, 432
3275.9	2054.3	1.00(5)	798, 1222
	1542.6	0.35(4)	1309
3421.5	2997.5	0.69(5)	424
3455.9	431.7	0.52(11)	424, 453, 767, 882, 917, 2571
3602.6	3602.8	3.4(7)	
	3178.3	9.4(11)	424
	1498.4	0.32(4)	1680
	1463.0	0.39(8)	798,918
	1270.1	0.37(3)	346, 424, 1908, 2333
3636.2	3636.1	0.75(14)	

Table 1: (continued)

E_{level}(keV)	E_γ(keV)	Relative Intensity	Coincident lines
	3214.2	1.7(4)	424
3672.2	1567.8	0.84(5)	424, 882, 1680, 2104
	432.0	0.13(8)	424, 2816, 3242
3977.9	3978.2	0.9(4)	511
	3553.6	0.97(16)	424
3986.4	3562.7	1.1(2)	424
	3216.3	1.2(2)	346, 424
4026.5	4026.8	0.86(16)	424
	3602.2	1.7(4)	424
	3257.4	0.46(15)	346, 424
	2805.5	0.60(5)	424, 798, 1222
4097.6	4098.8	1.00(17)	
	3673.6	2.2(2)	424
	3327.6	0.29(8)	346
4289.3	2185.0	1.5(1)	424, 798, 882, 1334, 1680
	1718.6	2.7(1)	346, 424, 884,917, 2571
	686.5	0.39(3)	3178

2.1.2 Level lifetime measurements

Lifetimes of the excited states were measured by means of the Advanced Time-Delayed $\beta\gamma\gamma(t)$ method, which is described in more details in [17–19]. All lifetimes and lifetime limits were determined using the centroid shift method, which required a precise calibration of the time-response of the BaF_2 γ detector as a function of γ energy. This was done off-line at ISOLDE using long-lived sources of ^{140}Ba and ^{140}La, which lifetime values were taken from [20]. Further calibration of the detectors was done at the OSIRIS fission product mass separator at Studsvik in Sweden using various radioactive beams.

Figures 2 and 3 illustrate the basic ideas behind the centroid shift analysis used for ^{76}Kr. By comparison of the energy spectra recorded in the Ge and BaF_2 detectors, shown in middle and bottom panels in Fig. 2, one can note the ability to select uniquely the β-917-424 keV cascade. Namely, by gating on the 917-keV transition in the Ge detector one can uniquely select the 424 keV transition in the BaF_2 detector. Similarly (not shown in the figure), one can selects the β-1263-424 keV cascade, with the same 424 keV transition in the BaF_2 crystal.

Figure 4 shows two time-delayed spectra gated by the fast response β and BaF_2 detectors, where the same 424 keV transition is selected in BaF_2. The top spectrum is due to the β-917(Ge)-424(BaF_2) keV cascade, where the 917 keV transition was selected in the Ge detector. The spectrum in the bottom panel is due to the β-1263(Ge)-424(BaF_2) keV sequence, where the Ge gate is set on the 1263 keV transition. Since both the 917 and 1263 keV transitions de-excite the 1687 keV level, the respective time-delayed spectra have the same time-delayed components due to the β and γ feeding the level from above. Thus the difference in the centroids of these time-delayed spectra is identical except for the lifetime of the 0^+ 770 keV level, which causes an additional time delay of the first time spectrum.

This shift is well visible in these time spectra. The broken line in Fig. 4 (both panels) marks the centroid of the bottom time-spectrum, which is positioned visibly to the left of the centroid

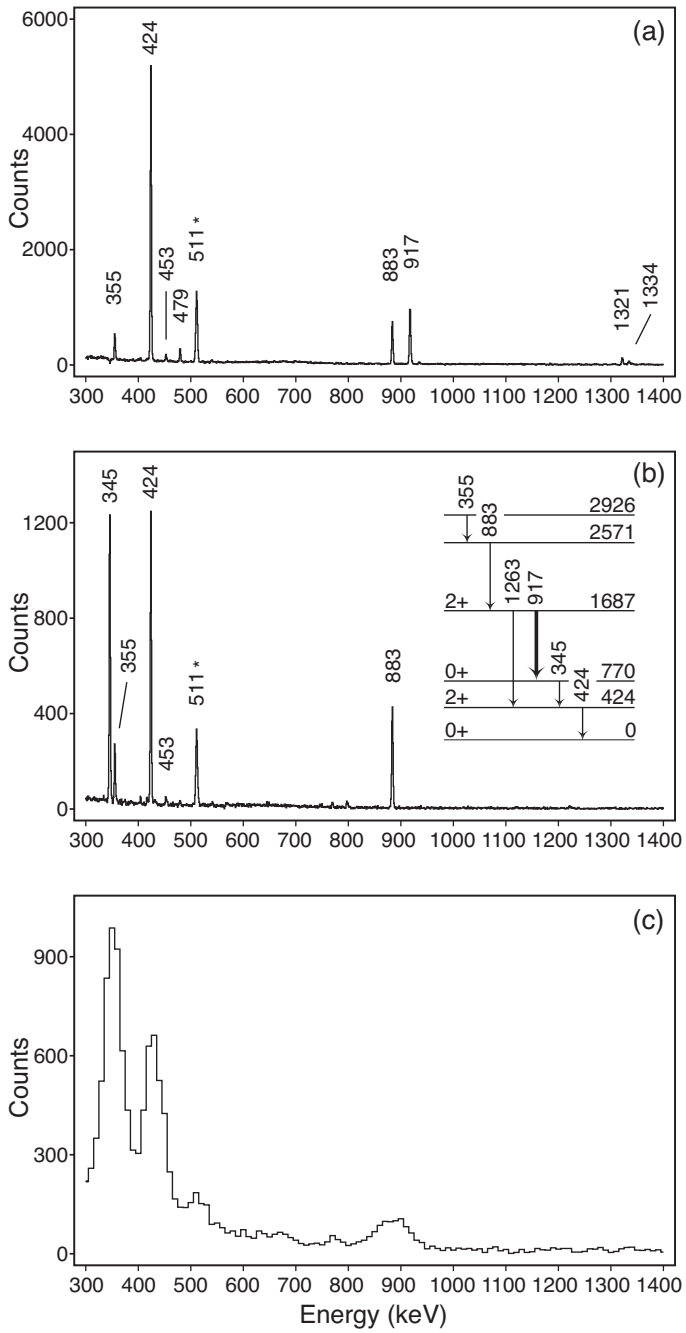

Fig. 2: Selected results from the $\beta\gamma\gamma$ coincidences using β-Ge-Ge and β-Ge-BaF_2 detectors. Top Panel: portion of the Ge energy spectrum in coincidence with the 345 keV transition. Middle and Bottom Panels: portion of the coincident Ge and BaF_2 energy spectra, respectively, gated on the 917 keV transition in Ge. The latter spectrum shows good separation of the 345, 424, 511 and 883 keV peaks. This is crucial in order to select the 345-424, 917-424, 917-345 time-delayed coincidences, which were used to determine the lifetime of the 0^+ 770 keV level; see text for details.

of the top panel time spectrum (the difference is about 2 channels). The observed time shift is 51(18) ps and it corresponds to the half-life of the 770 keV level of 35(12) ps. The final result of $T_{1/2}$=42.3(56) ps for the 0^+ 770 keV state listed in Table II, is a weighted average of many

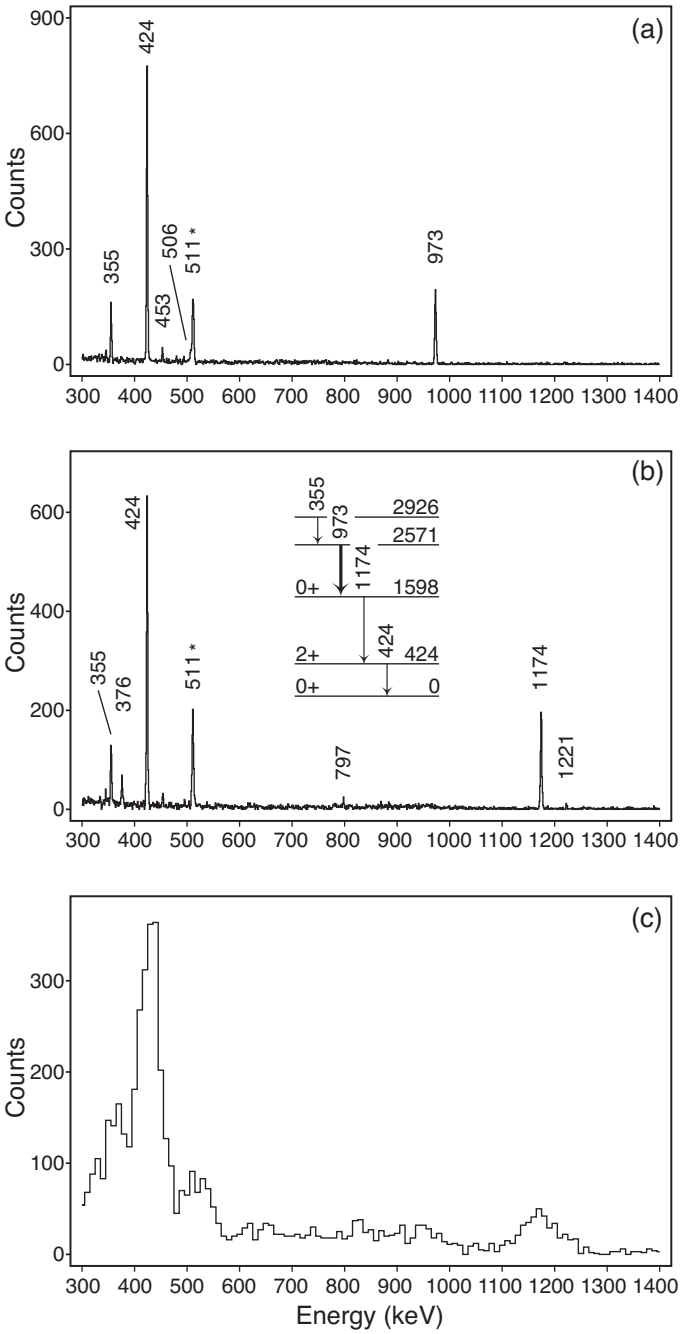

Fig. 3: Selected results from the $\beta\gamma\gamma$ coincidences using β-Ge-Ge and β-Ge-BaF_2 detectors. Top Panel: portion of the Ge energy spectrum in coincidence with the 1174 keV transition. Middle and Bottom Panels: portion of the coincident Ge and BaF_2 energy spectra, respectively, gated on the 973 keV transition in Ge. The latter spectrum shows good separation of the 355, 424, 511 and 1174 keV peaks. These spectra help to visualize the lifetime determination of the 0^+ 1598 keV state, see text for discussion.

results obtained using cascades passing through this level.

Figure 3 illustrates another way to get the lifetime of a level. This is using the idea of two γ rays, one feeding the level from above (the 973 keV transition) and the other de-exciting it (the

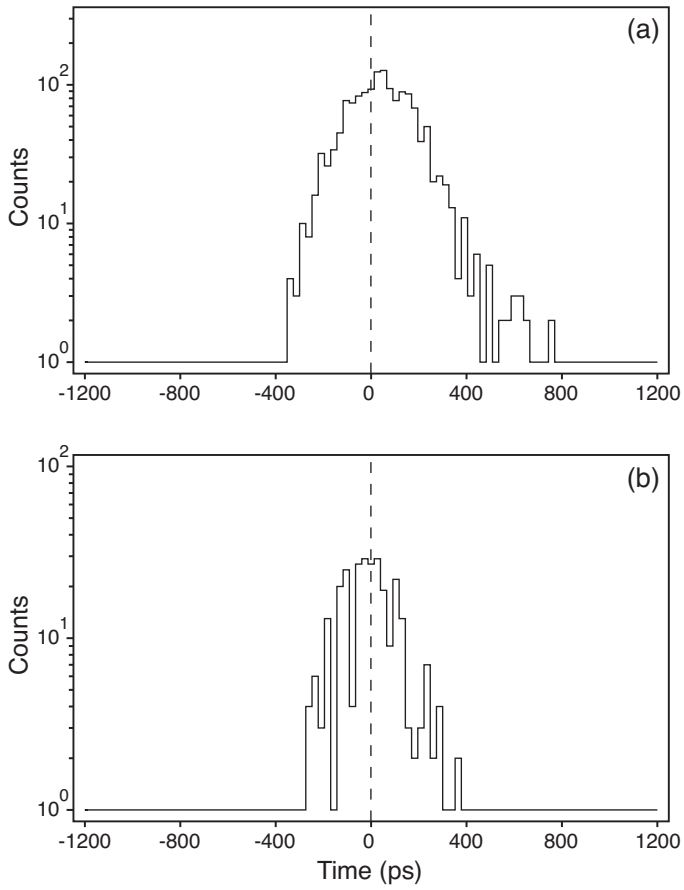

Fig. 4: Time-delayed $\beta\gamma$(t) spectra gated by the fast response β and BaF_2 detectors with the following gates: β-917(Ge)-424(BaF_2) in the Top Panel and β-1263(Ge)-424(BaF_2) in the Bottom Panel. The difference in the centroids is due to the lifetime of the 0^+ 770 keV level. The broken line marks the centroid of the bottom spectrum, from which the centroid of top spectrum is visibly shifted to the right. The observed time-shift is 51(18) ps and it corresponds to the half-life of the 770 keV level of 35(12) ps; see text for discussion. Time scale is 26.1 ps/ch.

1174 keV line). The time-delayed spectrum due to the β-973(BaF_2)-1174(Ge) keV cascade, provides the time reference point, from which the centroid of the β-973(Ge)-1174(BaF_2) keV time-delayed spectrum is shifted due to the lifetime of the 1598 keV state. In this case the time shift is very small and we determine only an upper limit of $T_{1/2} \leq 10$ ps. After averaging over values obtained from a few cascades passing via this level the final result listed in Table II is $T_{1/2} \leq 4.7$ ps.

In the centroid shift analysis corrections were made for the Compton contribution under the full energy peaks, including that of 511 keV, and for lifetimes of higher-lying levels. Only those results were considered where the corrections were small. Since the lifetimes of a number of excited states were of the order of a few to several picoseconds, the analysis has been made in a few steps. In the first one, the known lifetimes of the 424, 1034, 1221, and 1733 keV states have been used and the lifetimes of the other states were deduced by ignoring the small corrections due to the non-negligible lifetimes of the higher-lying levels. In the second step the analysis has been repeated but this time the corrections due to lifetimes of the higher-lying levels were made

Table 2: Experimental half-lives of the indicated levels deduced in this work.

E_{level}(keV)	$T_{1/2}$(ps)
770	42.3(56)
1598	< 4.7
1687	< 4.8
2091	< 34
2104	16.0(48)
2227	25.2(56)
2257	< 5.7
2571	16.1(43)
2700	< 27
2775	22(10)
2817	< 13
2927	20.7(54)
2970	< 39
3024	17.8(56)
3242	< 23
3421	< 24
3603	< 9.7
3978	< 17
3986	27(18)
4027	< 17
4098	< 18

using the lifetime values deduced in step one. Steps three and four represented a repetition of step two, each time using updated lifetime values. However, already after step three there were no meaningful changes in the deduced level lifetimes. The results of lifetime measurements are summarized in Table II.

2.2 K-conversion electron and γ-ray spectroscopy

Internal conversion electron and γ-ray measurements have been performed to deduce K-conversion coefficients of γ transitions, to possibly identify new excited 0^+ states besides the 0_2^+ state at 770 keV, and to study the decay of the 0^+ states. In addition, information from singles γ-ray spectra have been partially exploited in establishing the decay scheme (see next Section).

Conversion electrons were detected by means of a very compact magnetic transport system (whose basic components are described in detail in [22]), which can deflect electrons up to an energy of 3 MeV onto a 5 $cm^2 \times 6$ mm Si(Li) detector cooled to the liquid nitrogen temperature. An upgrading of the system [23] proved to be necessary to match the beam characteristics of the ISOLDE separator. The main changes were related to i) the construction of an electron suppressed Faraday cup of very small dimension to tune up the beam focusing at the collection point; ii) the employment of a moving tape system to collect ^{76}Rb nuclei at the target position (beam spot $\sim$ 3 mm diameter). The tape was moved every 20 minutes to a shielded site, to remove the β^+-EC activity of the ground state of ^{76}Kr [$T_{1/2} = 14.8$ h]; iii) the larger distance of the silicon detector to the collection point and the insertion of additional shielding to reduce the background due to gamma rays. The momentum acceptance of the system was $\Delta p/p = 18\%$

(Full Width Half Maximum) and the energy resolution of the detector was ∼2.2 keV for 1 MeV electrons. The energy calibration and the relative efficiency of the electron spectrometer as a function of the electron energy were obtained by using point electron sources of ^{207}Bi and ^{152}Eu placed at the collection point. The overall full energy peak efficiency turned out to be approximately constant at a value of about 0.3% over the $150 \div 1200$ keV energy range and to drop to about 0.1% at 1.8 MeV.

Gamma rays up to an energy of $\simeq$ 3 MeV were detected by a HPGe detector (having a resolution of 2.2 keV at 1.33 MeV energy) placed 100 cm away from the source to keep the counting rate at a typical value of about 10 kHz.

Gamma and electron spectra were recorded simultaneously by means of a multiplexed acquisition system. A computerized procedure was used to control irradiation and measure times, the movement of the tape, and the setting of different magnetic fields.

2.2.1 K-conversion coefficients

As a first step, the actual source position, which affects the proportionality constant connecting the magnetic field to the transmitted electron momentum, was checked. To this end the area of the K-conversion peak for the 424 keV, $2_1^+ \rightarrow 0_1^+$ transition was evaluated for electron energy spectra recorded at different magnetic field settings and normalized to the corresponding γ transition so as to determine the point of maximum transmission. Electron energy spectra were then recorded for several magnetic field settings corresponding to the maximum transmission of the electron lines of interest in the energy range $300 \div 1800$ keV.

The area of the electron lines, which have an asymmetric shape, were evaluated by fitting them with an "ad hoc" function, that has proven effective in previous work.

Internal conversion coefficients were determined through the Normalized Peak-to-Gamma (NPG) method [24]. The K-conversion coefficient of the reference line of known multipolarity was taken from [25]. When a reference line could be recorded simultaneously with the line of interest, its area has been corrected to compensate for the different transmission of the spectrometer at the two energies. In a few cases reference was made to the strong $2_1^+ \rightarrow 0_1^+$ transition recorded in a separated calibration run at the maximum of the transmission.

For some transitions connecting states of known spins and parity it has been possible to evaluate the mixing ratio δ^2. For $\delta^2(E2/M1)$ this was done by comparing the experimental value of the K-conversion coefficient with the value of α_K obtained from the expression

$$\alpha_K = \frac{\alpha_K(M1) + \delta^2\,\alpha_K(E2)}{(1+\delta^2)} \tag{1}$$

where $\alpha_K(M1)$ and $\alpha_K(E2)$ are the theoretical conversion coefficients [25]; for the mixing ratio $\delta^2(M2/E1)$ the analogous expression was used.

An example of the determination of $|\delta|$ is shown in Fig. 5.

The α_K^{exp} values are reported in Table III together with the theoretical ones [25]; the quoted errors correspond to one standard deviation. To give an idea of the internal consistency of the data, the K-conversion coefficient of the 346 keV transition, which has pure *E*2 multipolarity, is also reported. The deduced $|\delta|$ values are given in column (7). The information on spin-parity of the levels, shown in the last column, is deduced in most cases from the comparison of experimental and theoretical α_K. The experimental K-conversion coefficients of the 378, 686, and 1270 keV transitions from the 2571, 4289, and 3603 keV levels to the 2192, 3603 and 2333 keV levels, respectively, fix the negative parity of the final states.

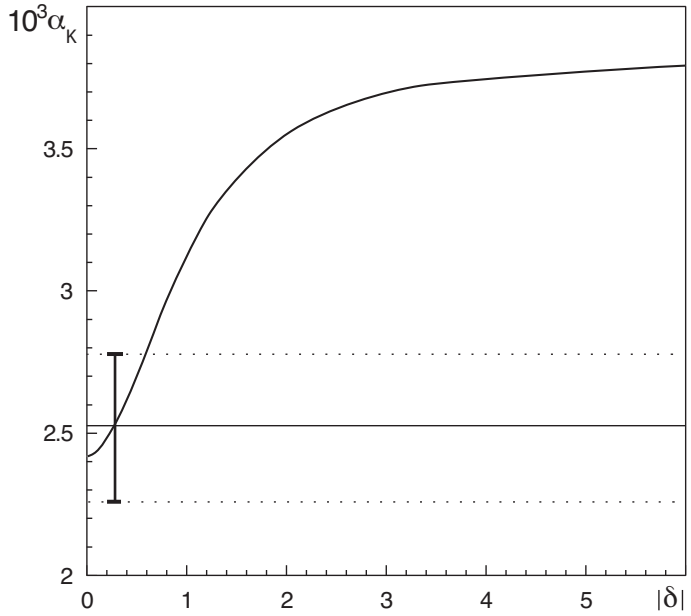

Fig. 5: The calculated value of α_K as a function of $|\delta|$ is compared to the experimental one for the 453 keV transition de-exciting the 3024 keV level. The error bar corresponds to one standard deviation.

The J$^\pi$ = 0^+ assignment to the 1598 keV level is based on arguments presented in the next subsection; one can notice that the K-conversion coefficient values of the two transitions de-exciting this level are in agreement with such an assignment.

2.2.2 E0 transitions

Measurements of conversion electrons can provide information on the decay properties of 0^+ states through the determination of the intensity ratio $q^2_{ifj} = I_K(0^+_i \rightarrow 0^+_f)/I_K(0^+_i \rightarrow 2^+_j)$. One can deduce the ratio X_{ifj} of the electric monopole $B(E0; 0^+_i \rightarrow 0^+_f)$ to electric quadrupole $B(E2; 0^+_i \rightarrow 2^+_j)$ reduced transition probabilities via the expression [26]

$$X_{ifj} = 2.56 \cdot 10^9 A^{\frac{4}{3}} E^5_\gamma[\mathrm{MeV}] \, \frac{\alpha_K(E2) \cdot q^2_{ifj}}{\Omega_K[\mathrm{s}^{-1}]} \tag{2}$$

where Ω_K is the electronic factor for the K-conversion of the *E*0 transition (tabulated e.g. in [27]) and α_K is the K-internal conversion coefficient of the $0^+_i \rightarrow 2^+_j$ transition.

If the lifetime of the level is known, it is possible to deduce the electric monopole strength $\rho^2(E0; 0^+_i \rightarrow 0^+_f)$, which is related to q^2_{ifj} and to the lifetime τ of the 0^+_i level by the expression

$$\rho^2(E0; 0^+_i \rightarrow 0^+_f) = \frac{q^2_{ifj} \cdot \alpha_K(E2) \cdot b_j}{\Omega_K \cdot \tau} \tag{3}$$

where b_j is the branching of the 0^+_i state to the 2^+_j state.

Table 3: Experimental values of the K-internal conversion coefficients (in units of 10^{-3}) for the specified transitions are compared with the theoretical values [25] for *E*1, *M*1, *E*2 and *M*2 transitions. Energies of levels and transitions are given in keV. In columns (2) and (4) are reported the previously known [28] J^π of initial and final states. Absolute values of *E*2/*M*1 or *M*2/*E*1 mixing ratios δ deduced from α_K^{exp} are reported in column (11). Spin (or limits thereof) and parity assignments deduced from the conversion coefficient measurements are given in the last column.

E_i	J_i^π	E_f	J_f^π	E_γ	α_K^{exp}	$\alpha_K(E1)$	$\alpha_K(M1)$	$\alpha_K(E2)$	$\alpha_K(M2)$	$\lvert\delta\rvert$	J^π
770	0^+	424	2^+	346	9.30(33)			9.21			
1222	2^+	424	2^+	797	0.727(47)		0.677	0.771			
1598	(≤ 4)	424	2^+	1174	0.311(19)	0.141	0.299	0.307			0^+
		1222	2^+	376	5.0(14)	1.85	3.76	6.96			
1687	2^+	424	2^+	1263	0.278(30)		0.257	0.261			
1733	(3^+)	424	2^+	1309	0.222(39)	0.116	0.240	0.242			$2^+, 3^+, 4^+$
		1035	4^+	698	1.41(58)	0.400	0.903	1.09			
2091	(1,2^+)	770	0^+	1322	0.244(52)	0.114	0.235	0.237			$1^+, 2^+$
		1222	2^+	870	0.9(2)	0.253	0.564	0.623			
2104	(1,2^+)	424	2^+	1680	0.056(13)	0.0781	0.149	0.149		*E*1	$1^-, 2^-, 3^-$
2227	(2^-)	424	2^+	1803	0.088(18)	0.0703	0.132	0.131	0.245	$0.33^{+0.18}_{-0.33}$	$1^-, 2^-, 3^-$
2257	3^-	424	2^+	1834	0.071(21)	0.0686			0.236	$0.12^{+0.28}_{-0.12}$	
2571	(1,2^+)	1598	(≤ 4)	973	0.212(28)	0.201	0.442	0.472			1^-
		1687	2^+	884	0.213(18)	0.244	0.543	0.596		*E*1	
		2091	(1,2^+)	480	0.91(20)	0.957	2.12	3.22	7.05	< 0.17	
		2192		378	5(1)	1.83	3.71	6.84		$0.85^{+0.85}_{-0.50}$	
2927	(0,1,2)	2104	(1,2^+)	822	0.58(6)	0.283	0.633	0.712		[*M*1]	$0^-, 1^-, 2^-$
		2571	(1,2^+)	355	4.22(15)	2.16	4.31	8.41		< 0.12	
3024	(1^-,2)	2104	(1,2^+)	920	0.48(8)	0.225	0.498	0.540			$1^-, 2^-, 3^-$
		2257	3^-	767	0.89(17)	0.328	0.737	0.852			
		2571	(1,2^+)	453	2.52(26)	1.11	2.42	3.83		$0.28^{+0.30}_{-0.28}$	
3603		2333		1270	0.26(9)	0.122	0.254	0.258			$(\,)^-$
4289		2571	(1,2^+)	1718	0.16(6)	0.0755	0.144	0.143			$0^- \div 3^-$
		3603		686.3	1.0(3)	0.415	0.939	1.14			

To investigate the decay of the 0_2^+ state all electron spectra recorded at different magnetic field settings, in a range including that corresponding to the maximum transmission for the $0_2^+ \rightarrow 0_1^+$ transition, have been analyzed in order to reduce the statistical uncertainty on $I_K(0_2^+ \rightarrow 0_1^+)$. Since the intensities of the electron lines were derived from spectra recorded at different times, each electron spectrum was normalized to that of the simultaneously recorded $2_1^+ \rightarrow 0_1^+$ gamma transition. The spectrum recorded for maximum transmission of the $0_2^+ \rightarrow 0_1^+$ K-transition is shown in Fig. 6.

Besides determining the q_{211}^2 value, we checked whether additional 0^+ states could be identified. A careful inspection of the electron conversion spectrum recorded for a magnetic field setting corresponding to the maximum transmission for 810 keV electrons revealed the presence of a line at an energy of 813.9(3) keV (see Fig. 7), which could be the K-conversion line of a transition from the 1598.0(1) keV level to the 0_2^+, 769.9(1) keV level (see Table IV): indeed its energy is 14.2(3) keV lower than the energy difference between the levels ($\Delta E = 828.1(1)$ keV). This value closely matches the binding energy of a K-electron in krypton isotopes ($\epsilon_K = 14.3$ keV)

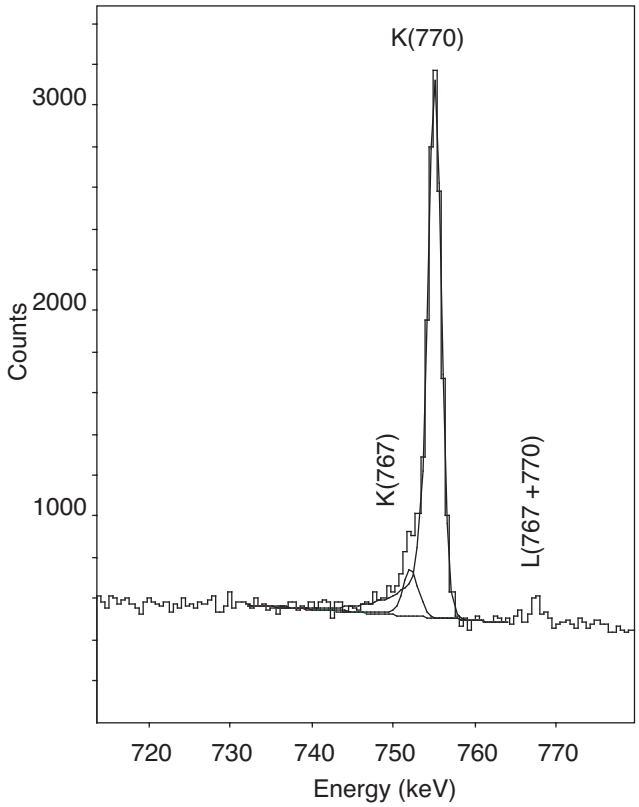

Fig. 6: Relevant section of an electron-energy spectrum showing the K- and L-conversion lines of the 770 keV, $0_2^+ \rightarrow 0_1^+$ transition. The two close lying K-770 keV and K-767 keV transitions (the latter de-excites the 3024 keV level) are clearly resolved by the fitting procedure.

and is incompatible with the ϵ_K of any other element. On the other hand no line is visible in the gamma spectrum at an energy of 828 keV; a very weak line could possibly be present at an energy of 827.2(3) keV. It should have at least a multipolarity 4 to be compatible with the observed intensity of the 813.9 keV electron line, which seems to be quite unlikely. We therefore assign spin J = 0 to the 1598 keV level.

To deduce the values of q^2_{321} and q^2_{322} we followed the same procedure as for q^2_{211}. It is to be noted that the intensity of the $0_2 \rightarrow 0_1$ and $0_3 \rightarrow 0_2$ K-transitions amounts to only 0.029% and 0.0002%, respectively, of that of the $2_1 \rightarrow 0_1$, 424 keV transition.

The values obtained for q^2_{ifj} and for the corresponding quantities X_{ifj} are reported hereafter:

$$\begin{aligned} q^2_{211} &= 0.203(8) \qquad X_{211} = 0.020(1) \\ q^2_{321} &= 0.11(2) \qquad X_{321} = 0.15(3) \\ q^2_{322} &= 0.09(3) \qquad X_{322} = 0.009(3) \end{aligned}$$

From the value of the lifetime of the 0_2^+ level and of the upper limit of the lifetime of the 0_3^+ level, the quantities

$$\begin{aligned} \rho^2(\mathrm{E0}; 0_2^+ \rightarrow 0_1^+) &= 0.079(11) \\ \rho^2(\mathrm{E0}; 0_3^+ \rightarrow 0_2^+) &> 0.007 \end{aligned}$$

have been derived. The quoted uncertainty on $\rho^2(\mathrm{E0}; 0_2^+ \rightarrow 0_1^+)$ corresponds to one standard deviation whereas the lower limit of $\rho^2(\mathrm{E0}; 0_3^+ \rightarrow 0_2^+)$ has been conservatively evaluated and corresponds to about two standard deviations.

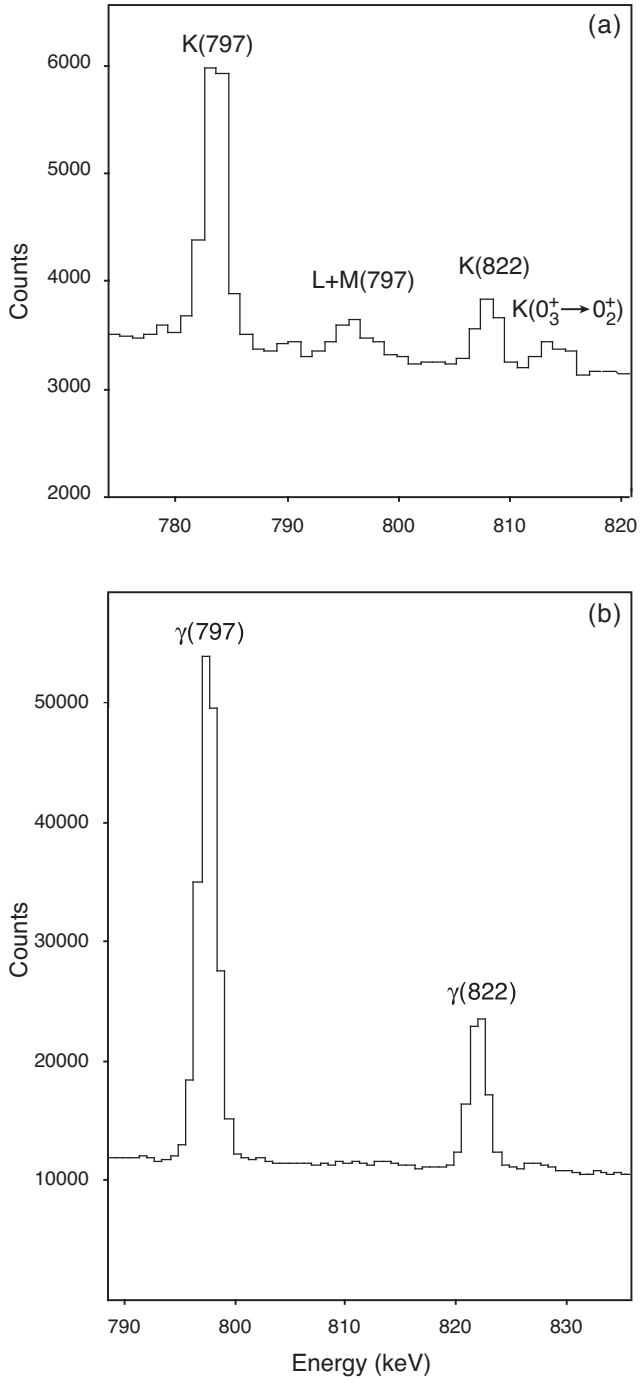

Fig. 7: Relevant sections of electron (a) and gamma (b) energy spectra showing the region around 800 keV. In the electron spectrum, in addition to the conversion lines of the 797 keV, $2_2^+ \rightarrow 2_1^+$ transition and 822 keV transition, de-exciting the 2104 keV level, a line at 814 keV is present with no counterpart in the gamma spectrum. It has been identified as the K-conversion line of the $0_3^+ \rightarrow 0_2^+$ transition (see text).

3 DECAY SCHEME

Previous studies on ^{76}Rb decay [29, 30] led to a decay scheme of ^{76}Kr comprising 16 levels up to an energy of $\simeq$ 3 MeV.

The present up-dated decay scheme is shown in Figs. 8, 9. It is based on the results of $\gamma - \gamma$ coincidences reported in Table I and γ-singles data. As a rule, transition energies and gamma-ray intensities have been deduced from the analysis of γ-singles spectra since, in this case, the distance of the germanium detector was large enough to exclude any influence of summing effects. The energies of some transitions which exceed 3 MeV were deduced from the corresponding single and double escape peaks. Whenever coincidence data indicated the presence of an unresolved doublet, intensity ratios were deduced from coincidence spectra. The side feeding of each level of ^{76}Kr populated in the decay of ^{76}Rb has been evaluated by a standard procedure. The corresponding log *ft* values were deduced by exploiting the usual practice [31] of utilizing the integral Fermi function (with Coulomb corrections) for allowed transitions [32]. Their values are reported in Fig. 8; the overall uncertainties of the reported values are estimated to be about $\pm$ 0.1.

The new spectroscopic information concerning i) excitation energies and transitions, ii) branching ratios, iii) spin-parity assignments, and iv) reduced transition probabilities is reported in Table IV together with previously available experimental data [28] on energies and spin-parity of levels.

i) All levels reported in [29] (including that at 2817 keV, not seen in [30]) have been observed in the present work. In addition, 7 levels and 22 transitions below 3 MeV and 12 levels (de-excited by 33 transitions) at higher energies have been identified. It is very likely that levels at 2700, 3241, and 3977 keV are the same observed in the (p,t) reaction [33] at 2697(15) [$J^\pi = 2^+$], 3246(15), and 3978(15) keV, respectively. The uncertainties on the energy of levels and transitions are only given for the new data since for the old ones our error estimate is very close to that reported in the literature [28].

Particularly difficult has been the placement of the 511.6 keV transition due to the presence of the very strong annihilation line. It has been assigned to the decay of the 1733.3 keV level since it appears in the spectrum gated by the 493.4 keV line (from the 2091 keV level) together with the 797.6 keV and 1309.3 keV transitions.

ii) A general satisfactory agreement exists with previous data [28] on the branching ratios, apart from a few cases concerning the levels at 1733, 2817, and 3024 keV. In particular, for the level at 2817 keV the $\gamma - \gamma$ coincidences revealed the presence of two transitions very close in energy (2816.6(4) keV and 2817.3(9) keV) de-exciting the levels at 2816.7 keV and at 3024 keV, respectively.

iii) The new spin-parity assignments, reported in column (5), are based on:

(a) the comparison between theoretical and experimental values of K-conversion coefficients (see Table III);

(b) the values of log *ft* from the present work. Restriction on the spin of the levels of the daughter nucleus have been derived according to the rules given in [34, 35]. We would like to remark that the log *ft* value of the transition populating the 2571 keV level [whose spin-parity has been deduced on the basis of argument (a)] allows to assign negative parity to the J =1 ground state of ^{76}Rb. This result is in agreement with the assignment suggested in [29]. For the level at 1733 keV, following [29], we adopt $J^\pi = 3^+$ even though arguments (a) and (b) would only restrict J^π to 2^+ and 3^+;

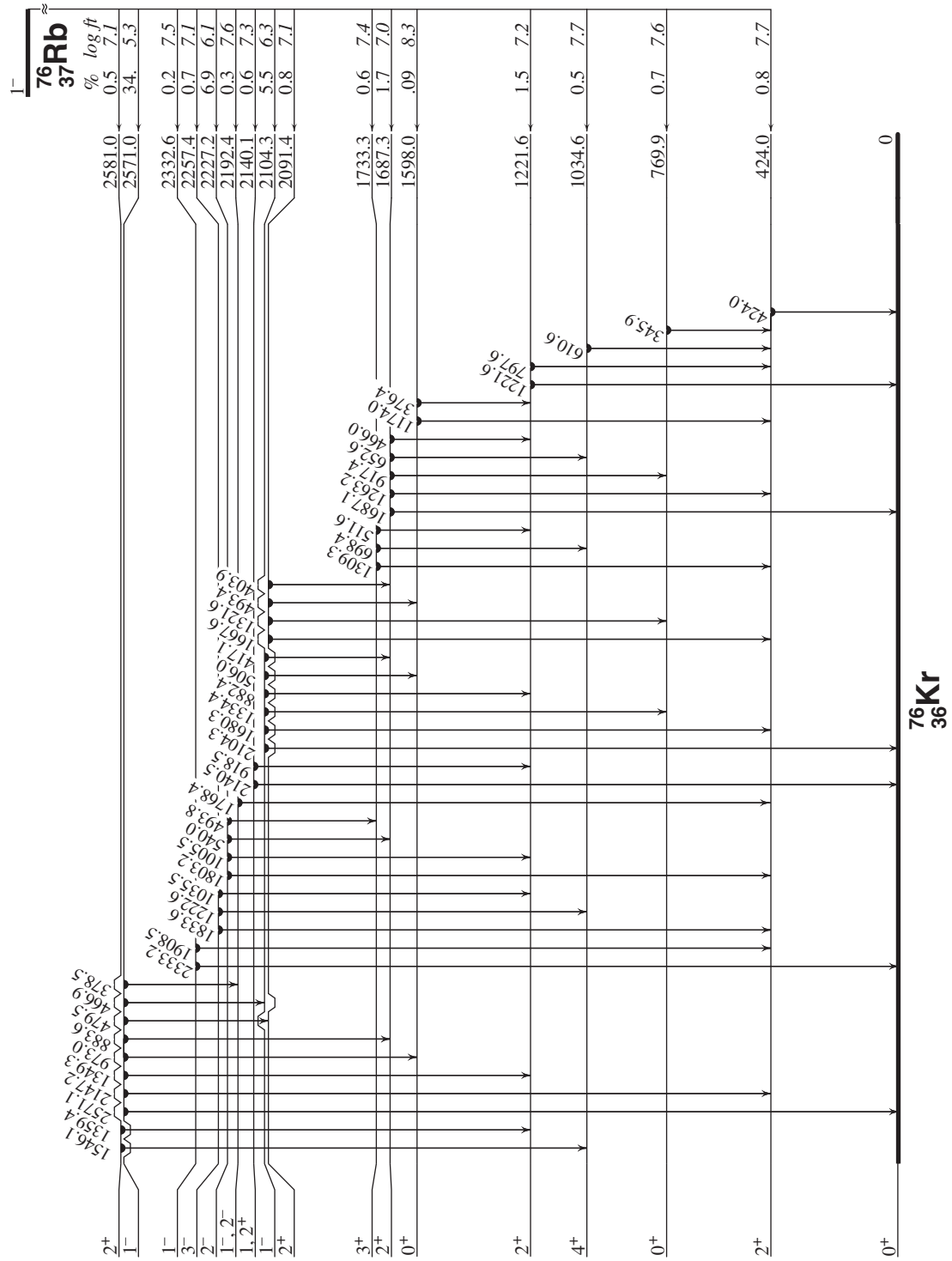

Fig. 8: Partial level scheme of ^{76}Kr showing the decay of the states populated in the β^+-decay of ^{76}Rb. The feeding percentage and the associated log *ft* values are reported on the right-hand side of the figure up to 2600 keV.

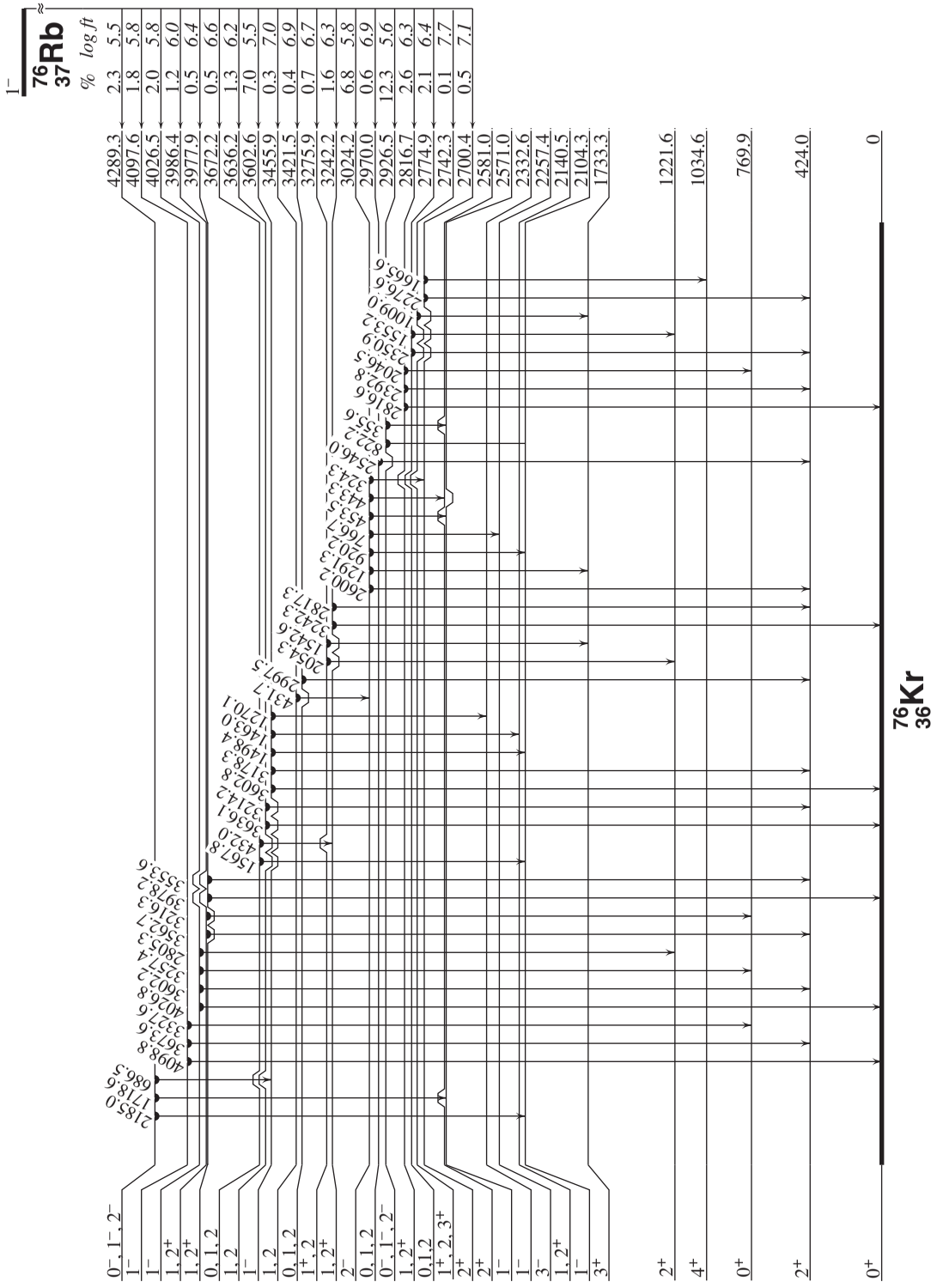

Fig. 9: Same as for Fig. 8 except for levels above 2600 keV.

(c) the assumption that the intensity of *M*2, *E*3, and *M*3 transitions is negligible compared to that of *E*1, *M*1, *E*2 transitions of similar energy de-exciting the same level. An internal consistency check of this hypothesis has been performed whenever possible (known level lifetime) by comparing the deduced partial lifetime with the recommended upper limits for the relevant multipolarities [36];

(d) additional arguments:

– the assignment $J^\pi = 2^+$ to the level at 2091 keV has been made combining the information ($J^\pi = 2^+$, 3^- or 4^+) from angular distribution measurements [33] with that from K-conversion coefficients, reported in Table III;

– on the basis of argument (a) the 2192 keV level has $J^\pi = 0^-, 1^-, 2^-$; the transition connecting the 2571 keV, 1^- level to the former state has a large *E*2 component (as it turns out from the measured $|\delta|$, see Table III) so that the value J = 0 can be excluded.

iv) Values (or limits thereof) for the reduced transition probabilities of several transitions of given multipolarity have been deduced from the level lifetimes measured in the present work; they are shown in column (8). Their values in Weisskopf units (W.u.) are given in the last column of the table.

4 DISCUSSION

4.1 0^+ states

A detailed analysis of the positive-parity states in even krypton isotopes has been recently performed by some of us [10] in the framework of the IBA-2 model. We therefore limit our discussion of positive-parity states in ^{76}Kr to the 0_2^+ and 0_3^+ states not considered in [10].

The interpretation of the nature of low-lying 0^+ states in even krypton isotopes, which has been the subject of several theoretical investigations, is still a matter of debate. For the particular case of ^{76}Kr, a large quadrupole deformation for the ground state was deduced [21, 37] from lifetime measurements [43], assuming an axially symmetric shape. It was explained by Piercey *et al.* [43] as due to the influence of the energy gaps in the single-particle Nilsson states for N, Z $\simeq$ 38 on nuclear shapes, which gives rise, in $^{76}_{36}\mathrm{Kr}_{40}$, to a prolate ground state. A near-spherical nature was instead attributed to the 0_2^+ state by Piercey *et al.* [21, 30] on the basis of the large energy spacings in the $(1, 2^+) \rightarrow 2_3^+ \rightarrow 0_2^+$, 884-917 keV cascade de-exciting the 2571 keV level compared to those of the $4_1^+ \rightarrow 2_1^+ \rightarrow 0_1^+$, 611-424 cascade. From the theoretical point of view, the coexistence of prolate and oblate or of prolate and spherical minima in ^{76}Kr are predicted by microscopic calculations [1, 3, 4]. Very recently, in the study of krypton isotopes through Coulomb excitation of radioactive krypton ion beams Korten *et al.* [38] found a prolate deformation of the ground state band in ^{76}Kr, with $\beta_2 = +0.38$.

To exploit the new information on 0^+ states collected in the present work we have compared the experimental data with the predictions based on a Schematic Two Levels model and the IBA-2 model.

Table 4: Spectroscopic data relative to levels in ^{76}Kr, populated in the β^+ decay of ^{76}Rb. Excitation energies and transition energies in columns (1) and (3) reported without error are taken from [28], those with the error are from the present work (except for the 1598 keV level, see text). Information on spin and parity shown in the second column is taken from [28]. Relative gamma intensities from each level, as determined in the present work, are given in the fourth column. Information deduced on spin and parity is reported in the fifth column; the letters in the comment column (6) refer to the arguments on which such assignments are based: (a) conversion coefficients results, (b) log*ft* values, (c) decay properties (see text), and (d) additional arguments. The multipolarity of the relevant transitions is shown in column (7). The values of the B(*E*1), B(*M*1), and B(*E*2) deduced from the half-lives shown in Table II, for transitions of known multipolarity, are reported in column (8) in units of $10^{-6}e^2$fm^2, $10^{-3}\mu_N^2$, and 10 e^2fm^4, respectively, and in the last column in Weisskopf units. In those cases where the *E*1 [*M*1] multipolarity is given in square brackets the corresponding B(*E*1) [B(*M*1)] has been evaluated assuming a negligible *M2* [*E2*] component.

E_{lev}(keV)	J^π	E_γ(keV)	%	J^π	Comm.	σ,λ	B(σ,λ)	B(σ,λ)$_{\rm W.u.}$
424.0	2^+	424.0	100(1)					
769.9	0^+	345.9	100(3)			*E*2	270(37)	138
1034.6	4^+	610.6	100(3)					
1221.6	2^+	1221.6	69(4)					
		797.6	100(3)					
1598.0(1)	(≤ 4)	1174.0	100(3)	0^+	d	*E*2	> 5.0	> 2.6
		376.4	8.1(4)			*E*2	> 120	> 61
1687.3	2^+	1687.1	28.8(10)			*E*2	> 0.15	> 0.08
		1263.2	21.2(7)					
		917.4	100(6)			*E*2	> 11	> 5.7
		652.6	9.2(3)			*E*2	> 5.6	> 2.9
		466.0	4.6(16)					
1733.3	(3^+)	1309.3	100(4)	3^+	a,b,d			
		698.4(1)	8.7(8)					
		511.6(2)	20(12)					
2091.4	(1,2$^+$)	1667.6	78.7(6)	2^+	a,d			
		1321.6	100(3)					
		493.4(1)	13.6(45)					
		403.9	20.7(11)					
2104.3	(1,2$^+$)	2104.3	16.0(5)	1^-	a,b,c	*E*1	0.30(9)	2.6 10^{-7}
		1680.3	100(3)			*E*1	3.7(11)	3.2 10^{-6}
		1334.4	7.0(3)			*E*1	0.51(16)	4.4 10^{-7}
		882.4(2)	21.8(46)			[*E*1]	5.6(21)	4.8 10^{-6}
		506.0(9)	7.3(27)			*E*1	10(5)	8.5 10^{-6}
		417.1(1)	2.0(2)			[*E*1]	4.7(15)	4.0 10^{-6}
2140.5(2)		2140.5(2)	26(3)	$1,2^+$	c			
		918.5(7)	100(33)					
2192.4(2)		1768.4(2)	100(6)	$1^-,2^-$	a,b			
2227.2	(2^-)	1803.2	100(3)	2^-	a,b,c	*E*1	2.3(5)	2.0 10^{-6}
		1005.5	19.1(6)			[*E*1]	2.6(6)	2.2 10^{-6}
		540.0(1)	2.2(2)			[*E*1]	1.9(5)	1.6 10^{-6}
		493.8(7)	6.4(18)			[*E*1]	7.1(28)	6.1 10^{-6}
2257.4	3^-	1833.6	100(3)			[*E*1]	> 9.0	> 7.7 10^{-6}

Table 4: (continued)

E_{lev}(keV)	J^π	E_γ(keV)	%	J^π	Comm.	σ,λ	B(σ,λ)	B(σ,λ)$_{W.u.}$
		1222.6(6)	26(15)			[$E1$]	$>$ 7.9(4)	$>$ 6.8 10^{-6}
		1035.5	11.8(9)			[$E1$]	$>$ 5.9(8)	$>$ 5.1 10^{-6}
2332.6(2)		2333.2(4)	31(8)	1^-	a,c			
		1908.5(2)	100(5)					
2571.0	(1,2^+)	2571.1	100(4)	1^-	a	$E1$	1.3(3)	1.1 10^{-6}
		2147.2	1.39(7)			[$E1$]	0.03(1)	2.6 10^{-8}
		1349.3	2.22(7)			[$E1$]	0.19(5)	1.7 10^{-7}
		973.0	6.1(2)			$E1$	1.4(4)	1.2 10^{-6}
		883.6	12.5(4)			$E1$	3.9(10)	3.4 10^{-6}
		479.5	2.25(8)			$E1$	4.5(12)	3.9 10^{-6}
		466.9(13)	0.3(1)					
		378.5(1)	0.70(3)			[$M1$]	0.25(7)	1.4 10^{-4}
2581.0(11)		1546.1(3)	47(19)	2^+	b,c			
		1359.4(1)	100(4)					
2700.4(3)		2276.6(4)	100(5)	2^+	b,c			
		1665.6(5)	25(4)			$E2$	$>$ 0.03	$>$ 1.7 10^{-2}
2742.3(2)		1009.0(2)	100(11)	$1^+, 2, 3^+$	b,c			
2774.9	($0^+, 1, 2$)	2350.9	100(4)	$0, 1, 2$	b			
		1553.2	56(3)					
2816.7	($1, 2^+$)	2816.6	$<$ 56	$1, 2^+$	b,c			
		2392.8	100(3)					
		2046.5(2)	30(2)					
2926.5	(0,1,2)	822.2	14(4)	$0^-, 1^-, 2^-$	a	$M1$	0.42(15)	2.4 10^{-4}
		355.5	100(3)			[$M1$]	37(10)	2.1 10^{-2}
2970.0(3)		2546.0(3)	100(6)	$0, 1, 2$	b			
3024.2	(1^-,2)	2600.2	61(2)	2^-	a,c	[$E1$]	0.32(10)	2.8 10^{-7}
		1291.3(3)	8.5(13)			[$E1$]	0.37(13)	3.2 10^{-7}
		920.2(1)	16.8(8)					
		766.7	56.6(17)					
		453.5	100(4)			[$M1$]	9(3)	5 10^{-3}
		443.3(1)	5.0(5)			[$E1$]	5.4(18)	4.6 10^{-6}
		324.3(1)	14.5(8)			[$E1$]	40(13)	3.4 10^{-5}
3242.2(3)		3242.3(3)	57(9)	$1, 2^+$	b,c			
		2817.3(9)	100(29)					
3275.9(2)		2054.3(5)	100(5)	$1^+, 2$	b,c			
		1542.6(2)	35(4)					
3421.5(5)		2997.5(5)	100(7)	$0, 1, 2$	b			
3455.9(5)		431.7(5)	100(21)	1,2	b,c			
3602.6(1)		3602.8(10)	36(7)	1^-	a,c	$E1$	$>$ 0.23(4)	$>$ 2.0 10^{-7}
		3178.3(2)	100(12)			[$E1$]	$>$ 0.95(6)	$>$ 8.1 10^{-7}
		1498.4(3)	3.4(4)					
		1463.0(2)	4.2(9)					
		1270.1(2)	4.0(3)					
3636.2(3)		3636.1(3)	44(8)	1,2	b,c			

Table 4: (continued)

E_{lev}(keV)	J^π	E_γ(keV)	%	J^π	Comm.	σ, λ	B(σ, λ)	B(σ, λ)$_{W.u.}$
		3214.2(14)	100(23)					
3672.2(2)		1567.8(2)	100(6)	$0, 1, 2$	b			
		432.0(9)	19(10)					
3977.9(3)		3978.2(4)	93(14)	$1, 2^+$	b,c			
		3553.6(4)	100(17)					
3986.4(3)		3562.7(4)	93(14)	$1, 2^+$	b,c			
		3216.3(4)	100(16)					
4026.5(3)		4026.8(6)	51(9)	1^-	b,c			
		3602.2(2)	100(24)					
		3257.4(5)	27(9)					
		2805.5(3)	32(3)					
4097.6(2)		4098.8(17)	46(8)	1^-	b,c			
		3673.6(2)	100(11)					
		3327.6(5)	13(4)					
4289.3(2)		2185.0(3)	55(3)	$0^-, 1^-, 2^-$	a,b			
		1718.6(4)	100(4)					
		686.5(4)	14.4(11)					

4.1.1 Schematic Two Levels model

As is well known, an important contribution to clarify the nature of the 0^+ states can be obtained from the analysis of *E*0 transitions, which are determined by a change in the radial distribution of electric charge inside the nucleus.

We followed the procedure (see, e.g., [14, 39–41]) of comparing the experimental value of $\rho^2(0_2^+ \rightarrow 0_1^+)$ with that evaluated in a simple mixing model where the 0_1^+ and 0_2^+ states are assumed to be linear combination of two basic configurations $|1>$ and $|2>$ of different deformations:

$|0_1^+> = b|1> + a|2>$ $\qquad$ $|0_2^+> = a|1> - b|2>$ $\qquad$ $(a^2 + b^2 = 1)$.

Starting from the expression of the monopole operator in terms of the deformation variables β and γ [42] it is possible to deduce an approximate expression for the monopole strength ρ^2

$$\begin{aligned} \rho^2(0_2^+ \rightarrow 0_1^+) &= (3Z/4\pi)^2 a^2(1-a^2)[(\beta(1)^2 - \beta(2)^2) \\ &+ (5\sqrt{5}/21\sqrt{\pi})(\beta(1)^3 cos(3\gamma(1)) - \beta(2)^3 cos(3\gamma(2))]^2 \end{aligned} \tag{4}$$

by neglecting the non-diagonal term $< 2|T(E0)|1>$ and keeping only terms up to the third order in β. Here $\gamma(1)$, $\beta(1)$ and $\gamma(2)$, $\beta(2)$ refer to the $|1>$ and $|2>$ states, respectively.

The value of $\rho^2(0_2^+ \rightarrow 0_1^+)$ has been calculated assuming a prolate configuration ($\gamma(1) = 0°$) for state $|1>$, with $\beta(1)$ = 0.33, and an oblate configuration ($\gamma(2) = 60°$) for state $|2>$. The chosen value of $\beta(1)$ is close to that found in [1] for the prolate minimum. The deformation parameter $\beta(2)$ has been varied in a reasonable range for different values of *a*. A prolate configuration for state $|2>$ has not been taken into account since no predictions exist of two competing prolate minima in this region. In the case considered, the wave functions of the two basic states are localized at different regions of the deformation coordinate space. Since their

overlap is very small, the non-diagonal term in (5) should not contribute significantly to the calculated value of ρ^2. The predicted values of ρ^2 are compared to the experimental one in Fig. 10.

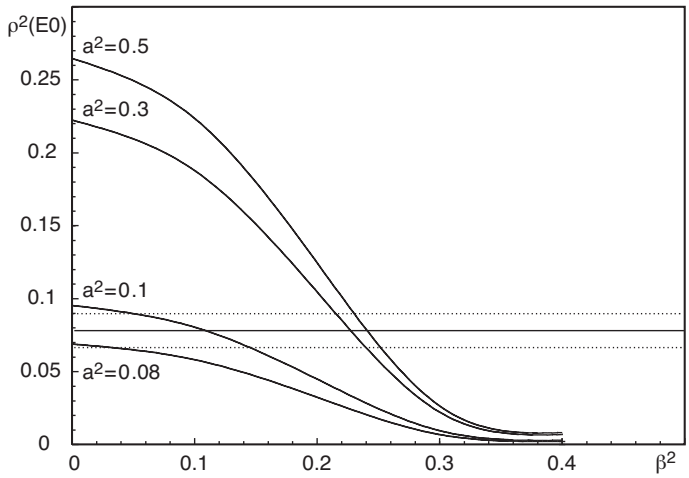

Fig. 10: Values of ρ^2 calculated as a function of the deformation parameter β_2 for different values of the squared mixing amplitude a^2, having assumed β_1 = 0.33. The horizontal lines indicate the experimental value together with the $\pm$ σ statistical uncertainty.

It is seen that the compatibility with the experimental value implies either a strong mixing and large $\beta(2)$ ($\simeq 0.24$) or a small mixing ($a^2 \simeq 0.1$) and near-spherical shape for the basis state $|2>$, therefore for the 0_2^+ state.

The first case, which could better explain the large observed B(*E*2; $0_2^+ \rightarrow 2_1^+$), is however incompatible with the results of (p,t) measurements [33] in which the 0_2^+ state was populated with an intensity of only 1% with respect to that of the ground state.

The second case corresponds to the interpretation given by Piercey [21, 30, 43] of shape coexistence due to a prolate deeper minimum competing with a spherical one. Although our assignment $J^\pi = 1^-$ to the 2571 keV level spoils the arguments (see above) given by Piercey *et al.* [21,30] on which this interpretation is based, such a shape coexistence would be in agreement with the recent findings [38] on the prolate deformation of the ground state band. It appears therefore that this interpretation is to be preferred even though the large value of the B(*E*2;$0_2^+ \rightarrow 2_1^+$) could raise some problem.

4.1.2 IBA-2 model

In the last two decades the nature of the 0_2^+ states along the Kr chain has been mainly investigated in the framework of the IBA model. In earlier analyses, in which only the energies of the levels were taken into account, these states were interpreted as "intruder" in [44] and as pertaining to the model in [6]. In subsequent IBA-2 analyses, where B(*E*2) reduced transition probabilities [7, 8] and *E*0 transitions [9] were also taken into account, the 0_2^+ states in $^{78-82}$Kr have again been considered to lie in the model space. Following the IBA-2 study carried out by some of us [9] on low-lying levels in $^{78-82}$Kr, a new analysis (not including excited 0^+ states) was performed [10] to study the positive-parity bands in $^{72-84}$Kr. A complete set of parameters for the whole isotopic chain was determined and a general good agreement between experimental and calculated data was obtained.

Table 5: Experimental data concerning the 0_2^+ states in $^{76-82}$Kr are compared to those calculated in the framework of the IBA-2 model by using the parameters of [10]; the *E*0 and *E*2 effective charges have the values β_ν = 0.25, β_π = 0.1 $e$fm^2 and e_ν =0.090, e_π = 0.075 eb, respectively. The energies are given in keV and the B(*E*2) in $10^{-3}e^2$b^2 units, the *E*0 strengths are reported as $\rho^2 \cdot 10^3$. Experimental data on the decay of the 0_2^+ states are taken from the following references: ^{76}Kr [present work], ^{78}Kr [9], ^{80}Kr [12], and ^{82}Kr [16].

	^{76}Kr		^{78}Kr		^{80}Kr		^{82}Kr	
	Exp	Calc.	Exp.	Calc.	Exp.	Calc.	Exp.	Calc.
E(2_1^+)	424	445	455	456	617	603	776	782
E(4_1^+)	1034	1059	1119	1072	1436	1356	1820	1707
E(0_2^+)	770	1075	1017	1086	1316	1320	1488	1642
B($E2;2_1^+ \rightarrow 0_1^+$)	164(6)	118	121(8)	96	73(4)	69	45(2)	50
B($E2;0_2^+ \rightarrow 2_1^+$)	270(37)	110	130(40)	89	70(30)	75	30(10)	59
$\rho^2(0_2^+ \rightarrow 0_1^+)$	79(11)	73	47(13)	60	21(9)	28	9(3)	11

However, as far as the 0_2^+ state are concerned, we note that the new experimental data on ^{72}Kr and ^{74}Kr [13–15] suggest that these states have to be considered outside the model space. In fact, the experimental energy differences E(0_2^+)$-$ E(2_1^+) in the two isotopes are equal to -402 keV and +52 keV, respectively, and are remarkably different from the corresponding calculated values which amount to +623 keV and +738 keV.

The experimental data relevant to the 0_2^+ state in $^{76-82}$Kr are compared in Table V with those calculated by using the parameters adopted in [10]. To give an idea of the agreement on excitation energies and transition strengths obtained in [10], the spectroscopic data relevant to the 2_1^+ and 4_1^+ states are also reported in the same table. The trend of $\rho_2^+(0_2^+ \rightarrow 2_1^+)$ values, steadily increasing from ^{82}Kr to ^{76}Kr, is correctly reproduced by the calculations. However, while in ^{78,80,82}Kr all the properties of the 0_2^+ state are satisfactorily reproduced, in ^{76}Kr the agreement is not so good for the excitation energy and the B($E2;0_2^+ \rightarrow 2_1^+$) so that no definite conclusion can be drawn on the collective character of this state.

As a result of the analyses using the Schematic Two Level model and the IBA-2 model it seems that no unique interpretation can be given to account for all experimental data. It is likely that in ^{76}Kr the structure of the 0_2^+ state (which is of predominant collective nature in the heavier isotopes) is determined by both collective and single particle degrees of freedom.

Finally, the level at 1598 keV has an energy very close to that predicted (1627 keV) for the 0_3^+ state. From the data reported in Table VI it is apparent that the calculations are not able to fully reproduce the experimental data. However, because of the remarks just made on the character of the 0_2^+ state and of the possible interaction between the two states, it is also difficult to draw any conclusion about the nature of the 0_3^+ state.

4.2 Negative-parity states

As shown in Figs. 8,9 several negative-parity states of spin ≤ 3 are populated in the decay of ^{76}Rb. Among them there is a group of five states whose energy ranges between 2.1 and 2.3 MeV. The 2258 keV, 3^- level is the only one among these states whose spin-parity was previously known. Gross *et al.* [37] found that this state is the bandhead of the negative-parity, odd-spin band, reported as based on the 5^- level in [21]; on the basis of calculations performed in the framework of the Woods-Saxon-Strutinsky cranking model these authors conclude that the band is most likely built on the $\pi[431]3/2^+ \otimes \pi[312]3/2^-$ Nilsson states. They also found that the level

Table 6: Experimental data on the 0_3^+ state in ^{76}Kr are compared to the calculated ones. The parameters used in the calculations and the units of the reported quantities are the same as in Table V.

	Exp.	Calc.
E(0_3^+)	1598	1627
X_{321}	0.147(26)	6.4
X_{322}	0.009(3)	0.047
$\rho^2(0_3^+ \rightarrow 0_2^+)$	> 7	96
B($E2$;$0_3^+ \rightarrow 2_1^+$)	> 5	0.5
B($E2$;$0_3^+ \rightarrow 2_2^+$)	> 120	68

at 2227 keV (for which they proposed $J^\pi = 2^-$) is the lowest state of a band previously observed to be based on the (4^-) state, for which even spin and negative parity were suggested [21, 45]. A two quasiparticle structure was considered also in this case as the most likely. These two bands have been further investigated in [46] in the framework of the quasiparticle random-phase approximation, which predicts very weak collectivity for the bandheads, and in [47], in the framework of a deformed configuration mixing shell model, where a satisfactory agreement for the excitation energies was obtained. Our definite assignment of $J^\pi = 2^-$ to the 2227 keV level provides a sound reference point for the mentioned calculations.

In addition to the 1^- states around 2.2 MeV excitation energy, four additional 1^- states have been identified at 2571, 3602, 4026, 4097 keV. We have considered the possibility that one of them could be the lowest 1^- collective state predicted by the IBA model [11]. No one of their energies, however, matches the expected one which is close to the sum of the energies of the lowest 2^+ and 3^- collective states ($\simeq 2.9$ MeV [48]). Besides, the B($E1$) values of the transitions de-exciting these states are at least two order of magnitude smaller than those expected ($10^{-3} - 10^{-4} e^2$fm^2 [49]) for the collective 1^- state.

5 CONCLUSIONS

The study of the ^{76}Rb decay, performed via fast timing, conversion electron and γ-ray spectroscopy, allowed us to extend the knowledge of the excitation energy pattern of ^{76}Kr up to about 4.5 MeV. Several new levels (and transitions) have been identified and for many of them lifetimes and spins and/or parities have been determined.

Of particular interest is the identification of the third 0^+ state and the study of the decay properties of the 0_2^+ and 0_3^+ states. The experimental value of $\rho^2(E0; 0_2^+ \rightarrow 0_1^+)$ has been compared to that calculated in a simple two-states mixing model. The properties of the 0_2^+ and 0_3^+ states have been investigated in the framework of the IBA-2 model. It turns out that no unique description is able to match all experimental data concerning the 0_2^+ state. It is likely that both single-particle and collective degrees of freedom take part in determining its character. The uncertainty on the nature of the 0_2^+ state and on its possible interaction with the 0_3^+ state makes also difficult to understand the structure of the latter.

As to the negative-parity states, we would like to stress that three out of the six 1^- states identified in this work are below 2.6 MeV. To our knowledge, no 1^- state has yet been observed (see Data Base of the National Nuclear Data Center, BNL) below 2.9 MeV in even-even nuclei of this mass region (Z = 32 $\div$ 40). The present $J^\pi = 2^-$ assignment to the 2227 keV level supports the hypothesis [21, 37, 45] of negative parity and even spin for the band built on this state.

Finally, the strong β^+ branching to the 2571 keV state (for which we assigned $J^\pi = 1^-$) allowed us to deduce a negative parity for the J =1 ^{76}Rb ground state.

ACKNOWLEDGEMENTS

Many thanks are due to P.G. Bizzeti and G. Lhersonneau for very helpful discussions. One of us (L.M.F.) would like to thank the OSIRIS group at Studsvik for their support and for their hospitality during his stay at INF. He would also like to acknowledge the support of the "Margit & Folke Pehrzon Foundation". This work was supported in part by the Swedish Research Council, the Spanish C.I.C.Y.T. under contracts AEN94–0833-C02–02, the Norwegian Research Council and the Polish Scientific Research Committee.

REFERENCES

[1] W. Nazarewicz, J. Dudek, R. Bengtsson, I. Ragnarsson, Nucl. Phys. **A435**, 397 (1985).

[2] P. Bonche, H. Flocard, P.H. Heenen, S.J. Kreiger, M.S. Weiss, Nucl. Phys. **A443**, 39 (1985).

[3] P. Sarriguren, E. Moya de Guerra, A. Escuderos, Nucl. Phys. **A658**, 13 (1999).

[4] A. Petrovici, J. Phys. G: Part. Phys. **25**, 803 (1999).

[5] A. Petrovici, K.W. Schmid, Amand Faessler, Nucl. Phys. **A665**, 333 (2000).

[6] K.I. Erokhina, A.D. Efimov, I.Kh. Lemberg, A.K. Vlasmikov, and V.M. Mikhilov, Izv. Akad. Nauk. SSSR, Ser. Fiz **48**, 328 (1984).

[7] A.F. Barfield and K.P. Lieb, Phys. Rev. C **41**, 1762 (1990).

[8] H. Dejbakhsh, A. Kolomiets, and S. Shlomo, Phys. Rev. C **51**, 573 (1995).

[9] A. Giannatiempo, A. Nannini, A. Perego, P. Sona, M.J.G. Borge, O. Tengblad, and the ISOLDE Collaboration, Phys. Rev. C **52**, 2444 (1995).

[10] A. Giannatiempo, A. Nannini, and P. Sona, Phys. Rev. C **62**, 044302 (2000).

[11] F. Iachello and A. Arima, *The Interacting Bosons Model*, (Cambridge University Press, Cambridge, England, 1987).

[12] A. Giannatiempo, A. Nannini, A. Perego, P. Sona, M.J.G. Borge, K. Riisager, O. Tengblad and ISOLDE Collaboration, Phys. Rev. C **47**, 521 (1993).

[13] E. Bouchez *et al.*, Phys. Rev. Lett. **90**, 082502 (2003).

[14] C. Chandler *et al.* Phys. Rev. C **56** R2924 (1997).

[15] F. Becker *et al.* Eur. Phys. J. A **4**, 103 (1999).

[16] A. Zemel, T. Hageman, J.J. Hamill, and J. van Klinken, Phys. Rev. C **31**, 1483 (1985).

[17] H. Mach, R.L. Gill and M. Moszyński, Nucl. Instrum. Methods **A280**, 49 (1989).

[18] H. Mach, F.K. Wohn, G. Molnár, K. Sistemich, J.C. Hill, M. Moszyński, R.L. Gill, W. Krips and D.S. Brenner, Nucl. Phys. **A523**, 197 (1991).

[19] M. Moszyński and H. Mach, Nucl. Instrum. Methods **A277**, 407 (1989).

[20] H. Mach and B. Fogelberg, Physica Scripta T **56**, 270 (1995).

[21] R. B. Piercey, A. V. Ramayya, J.H. Hamilton, X.J. Sun, Z.Z. Zhao, R.L. Robinson, H.J. Kim, and J.C. Wells, Phys. Rev. C **25**, 1941 (1982).

[22] T. Fazzini, A. Giannatiempo, A. Perego, Nucl. Instrum. Methods **211**, 125 (1983).

[23] P. Del Carmine, A. Giannatiempo, A. Nannini, M. Ottanelli, P. Pecchioli, and A. Perego, DFF311 - 6/98

[24] J.H. Hamilton, in *The Electromagnetic Interaction in Nuclear Spectroscopy*, edited by W.D. Hamilton (North-Holland, Amsterdam, 1975), p. 447.
[25] F. Rösel, H.M. Fries, K. Alder, and H.C. Pauli, At. Data Nucl. Data Tables **21**, 91 (1978).
[26] A.V. Alduschenkov and N.A. Voinova, Nucl.Data Tables **11**, 229 (1973).
[27] D.A. Bell, C.E. Aveledo, M.G. Davidson, and J.P. Davidson, Can. J. Phys. **48**, 2542 (1970).
[28] B. Singh, Nucl. Data Sheets 74, 63 (1995).
[29] D.M. Moltz, K.S. Toth, F.T. Avignone III, H. Noma, B.D. Kern, R.E. Tribble, and J.P. Sullivan, Nucl. Phys. **A427**, 317 (1984).
[30] R.B. Piercey, A.C. Rester, J.H. Hamilton, A.V. Ramayya, H.K. Carter, R.L. Robinson, H.J. Kim, J.C. Wells, and J. Lin, Phys. Rev. C **32**, 625 (1985).
[31] R.B. Firestone, Table of Isotopes, edited by V.S. Shirley (John Wiley & Sons Inc., 1996).
[32] N.B. Gove and M.J. Martin, Nucl. Data Tables **10**, 206 (1971).
[33] S. Matsuki, N. Sakamoto, K. Ogino, Y. Kadota, T. Tanabe, and Y. Okuma, Nucl. Phys. **A370**, 1 (1981).
[34] S. Raman and N.B. Gove, Phys. Rev. C **7**, 1995 (1973).
[35] B. Singh, J.L. Rodriguez, S.S.M. Wong, and J.K. Tuli, Nucl. Data Sheets 84, 487 (1998).
[36] P.M. Endt, Atomic Data and Nucl. Data Tables **23**, 547 (1979).
[37] C.J. Gross *et al.*, Nucl. Phys. **A501**, 367 (1989).
[38] W. Korten *et al.*, Nucl. Phys. **A746**, 90c (2004).
[39] K. Heyde and R.A. Meyer, Phys. Rev. C **37**, 2170 (1988).
[40] H. Mach, M. Moszynski, R. L. Gill, G. Molnar, F. K. Wohn, J.A. Winger, and J. C. Hill, Rev. C **42**, 793 (1990).
[41] J.L. Wood, E.F. Zganjar, C. De Coster, and K. Heyde, Nucl. Phys. **A651**, 323 (1999) and references therein.
[42] A.S. Davydov, V.S. Rostovsky, and A.A. Chaban, Nucl. Phys. **27**, 134 (1961).
[43] R. B. Piercey *et al.*, Phys. Rev. Lett. **47**, 1514 (1981).
[44] U. Kaup, A. Gelberg, Z. Phys. A **293**, 311 (1979).
[45] M.S. Kaplan, J.X. Saladin, L. Faro, D.F. Winchell, H. Takai, and C.N. Knott, Phys. Lett. B **215**, 251 (1988).
[46] T. Nakatsukasa, K. Matsuyanagi, I. Hamamoto, and W. Nazarewicz, Nucl. Phys. **A573**, 3334 (1994).
[47] K.C. Tripaty and R. Sahu, J. Phys. G: Nucl. Part. Phys. **26**, 1271 (2000).
[48] S. Matsuki, K. Ogino, Y. Kadota, N. Sakamoto, T. Tanabe, M. Yasue, A. Yokomizo, S. Kubono, and Y. Okuma, Phys. Lett. B **113**, 21 (1982).
[49] W. Andrejtscheff, C. Kohstall, P. von Brentano, C. Fransen, U. Kneissl, N. Pietralla, H.H. Pitz, Phys. Lett. B **506**, 239 (2001).